RL-TR-96-240
Final Technical Report
February 1997

THEORETICAL FOUNDATION OF HIGH-FREQUENCY MICROWAVE MODULATION OF LASER DIODES WITH SHORT EXTERNAL CAVITY

Rochester Institute of Technology

Dr. Guifang Li

APPROVED FOR PUBLIC RELEASE; DISTRIBUTION UNLIMITED.

Rome Laboratory
Air Force Materiel Command
Rome, New York

This report has been reviewed by the Rome Laboratory Public Affairs Office (PA) and is releasable to the National Technical Information Service (NTIS). At NTIS it will be releasable to the general public, including foreign nations.

RL-TR-96-240 has been reviewed and is approved for publication.

APPROVED:

STEVEN JOHNS
Project Engineer

FOR THE COMMANDER:

DONALD W. HANSON, Director
Surveillance & Photonics Directorate

If your address has changed or if you wish to be removed from the Rome Laboratory mailing list, or if the addressee is no longer employed by your organization, please notify RL/OCPC, 25 Electronic Pky, Rome, NY 13441-4514. This will assist us in maintaining a current mailing list.

Do not return copies of this report unless contractual obligations or notices on a specific document require that it be returned.

REPORT DOCUMENTATION PAGE

Form Approved
OMB No. 0704-0188

1. AGENCY USE ONLY *(Leave blank)*	2. REPORT DATE	3. REPORT TYPE AND DATES COVERED
	February 1997	**FINAL, May 95 - Dec 95**

4. TITLE AND SUBTITLE
THEORETICAL FOUNDATION OF HIGH-FREQUENCY MICROWAVE MODULATION OF LASER DIODES WITH SHORT EXTERNAL CAVITY

5. FUNDING NUMBERS
C - F30602-95-C-0091
PE - 62702F
PR - 4600
TA - P2
WU - PU

6. AUTHOR(S)
Dr. Guifang Li

7. PERFORMING ORGANIZATION NAME(S) AND ADDRESS(ES)
Rochester Institute of Technology
75 Highpower Rd
Rochester NY 14623

8. PERFORMING ORGANIZATION REPORT NUMBER
N/A

9. SPONSORING / MONITORING AGENCY NAME(S) AND ADDRESS(ES)
Rome Laboratory/OCPC
25 Electronic Pky
Rome NY 13441-4515

10. SPONSORING / MONITORING AGENCY REPORT NUMBER
RL-TR-96-240

11. SUPPLEMENTARY NOTES
Rome Laboratory Project Engineer: Steven T. Johns, OCPC, (315) 330-4456

12a. DISTRIBUTION AVAILABILITY STATEMENT
Approved for Public Release; Distribution Unlimited

12b. DISTRIBUTION CODE

13. ABSTRACT *(Maximum 200 words)*
In simulations, short external cavity laser diodes have shown to produce high frequency oscillations (>20Hz). This paper presents theoretical and simulated dynamics for such types of laser systems. The high frequency oscillations are a result of self twin-mode locking. It will be shown the critical feedback parameters and the frequencies of self twin-mode locking oscillations in these regimes of high frequency microwave oscillations are possible.

14. SUBJECT TERMS
high frequency microwave modulation, short-external cavity, semiconductor laser diodes

15. NUMBER OF PAGES
52

16. PRICE CODE

17. SECURITY CLASSIFICATION OF REPORT	18. SECURITY CLASSIFICATION OF THIS PAGE	19. SECURITY CLASSIFICATION OF ABSTRACT	20. LIMITATION OF ABSTRACT
UNCLASSIFIED	**UNCLASSIFIED**	**UNCLASSIFIED**	**UNLIMITED**

NSN 7540-01-280-5500

Standard Form 298 (Rev. 2-89)
Prescribed by ANSI Std. Z39-18
298-102

Table of Contents

Abstract

The dynamic properties of semiconductor laser diodes are significantly affected by external optical feedback. In this paper we present theoretical and simulated dynamics for a laser diode with a short external cavity. We assume that only the emitted photons are fedback only once by the external cavity. In the unstable regime of short external cavity laser diode operation high frequency oscillations (>20 GHz) exist as a result of self twin-mode locking. This instability corresponds to equalization of the cavity loss for the main mode (the lasing frequency) and sidemode. We will show the critical feedback parameters and the frequencies of self twin-mode locking oscillations in these regimes of high frequency microwave oscillations. As will be shown, both the Fabry-Perot and vertical cavity surface emitting lasers exhibit such microwave oscillations. The frequency-modulated microwave oscillation will be useful for all-optical high-speed transmitters.

1.0 Introduction

Semiconductor laser diodes exposed to optical feedback have been found to improve laser frequency stability and to narrow laser linewidth. Optical feedback, however, can also significantly change LD (laser diode) dynamics.

It also has been theoretically and experimentally demonstrated that the effects optical feedback vary with the external cavity length and with power feedback ratio. For long (~1cm and more) external cavity LD, these changes lead to chaotic self-modulation of laser light with dramatic increase in laser spectrum width and noise, instead of line narrowing (" coherence-collapse " effect [1]). It occurs as a result of sustained relaxation oscillations of laser output, when feedback coefficient exceeds some very low critical value about -40 dB and extends over several decades. This "coherence-collapse" regime was shown to be the result of a combined effect of the LD relaxation resonance and EC resonances [2] . For the short external cavity LD (SEC LD), the EC mode spacing is much larger than the LD relaxation frequency [4]. The larger mode spacing lend to avoid coherence-collapse.

In the unstable regime, a SEC LD exhibits high-frequency instability associated with locking of compound cavity modes for relative high values of coupling coefficients. This effect enables to achieve frequencies of optical current-controlled oscillators in excess of 20 GHz.

We can use SEC LD to generate tunable microwave oscillators with frequency modulation capacities. The frequency can be modulated by several ways. From our simulation result, we can modulate the frequency by changing optical feedback and the external cavity length.

In the following, we focus first on the theory of SEC LD including rate equation, steady state analysis and linear stability analysis. We introduce the Lang and Kobayashi rate equations for the SEC LD [3]. The steady state analysis shows that for each state of lasing the "steady-state" condition of instability occurs when the cavity losses for the main and side mode are equal [4]. Also, the linear stability analysis can predict the dynamic instability of laser operation caused by the twin-mode competition.

Furthermore, we use computer simulation to prove the instability. First, Fabry-Perot laser diodes with 200 um cavity length is used for computer simulation. Second, we use vertical-cavity surface emitting lasers (VCSEL) with 1 um cavity length for simulation. The structure of VCSEL is shown in Fig. 1 [5].

Compared with long cavity length, the advantage of the VCSEL is, due to its short cavity length, the longitudinal cavity mode spacing (being equal to c/2d , d is the cavity length) is very large. In fact, it is possible to have a mode spacing larger than the gain bandwidth of the active material. Thus, it can be inherently single longitudinal mode.

Finally, our results are summerized.

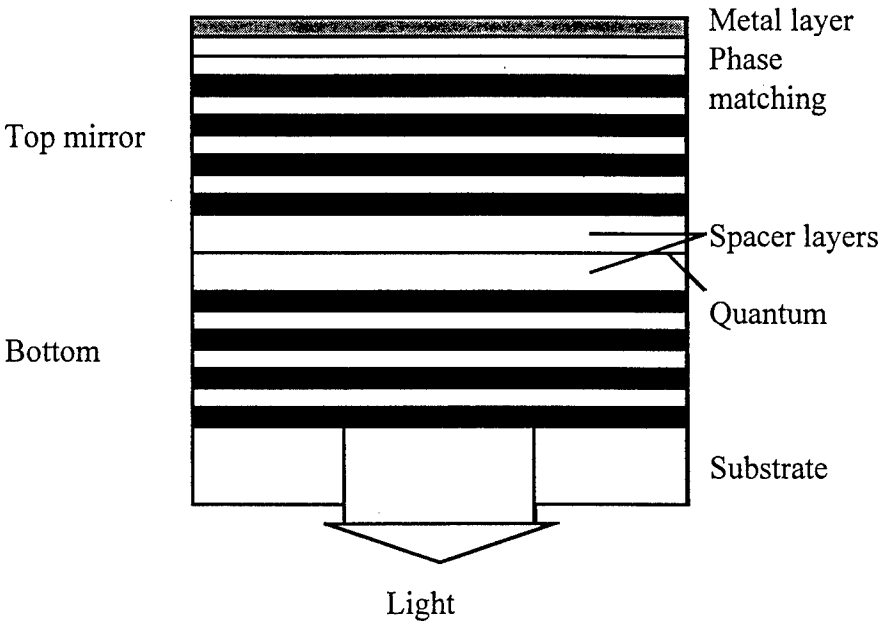

Fig.1 Schematic cross-section view of VCSEL structure considered here.

considered here.

2.0 Theory

2.1 Rate Equation

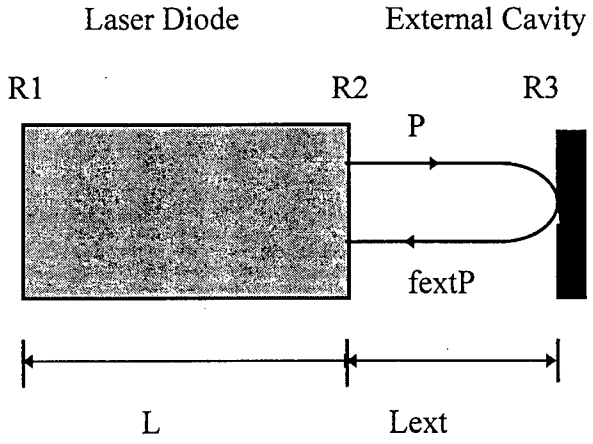

Fig. 2 Schematic of a laser diode with an external cavity

The schematic of a semiconductor laser diode with an external cavity is shown in Fig.2 . R1 and R2 are the reflectivity of the laser facets and R3 is the reflectivity of the external mirror. L and Lext are the lengths of the laser diode cavity and the EC; fext is the feedback. We will consider $\tau\omega_R << 1$, where $\tau = 2L_{ext}/c$ is the photon round-trip time in EC and ω_R is the angular frequency of the relaxation oscillation .

Here we use Lang and Kobayashi rate equations for the SEC LD. There are several assumptions for these rate equations. First, the solitary laser is assumed to be single mode, which implies $\tau >> \tau_0$ ($\tau_0 = 2Ln_g/c$, is the photon round-trip time in the LD-cavity. n_g is the group refraction index of the LD.) ; second, $f_{ext} << 1$ which means only one round-trip of the emitted photons is significant inside the EC. Then we arrive at the following two rate equations :

$$\frac{dE(t)}{dt} = j\left[\Omega_s - \Omega + \frac{\alpha}{2} g_N (N - N_s)\right]E(t) + \frac{1}{2}(g - \frac{1}{\tau_p})E(t) + \kappa E(t-\tau)\exp(-i\Omega\tau) \quad (1)$$

$$\frac{dN}{dt} = J - \frac{N}{\tau_{sp}} - gS \quad (2)$$

where $g = g(N)(1 - \kappa_p P)$ is the nonlinear gain where the linear gain is given by $g(N) = g_N(N - N_s)$; P is the output power.
Ω_s is the resonance optical frequency of the LD without EC.
α is the linewidth enhancement factor; g_N is the differential gain.

τ_p is the photon lifetime in the LD cavity.
τ_{sp} is the carrier lifetime due to spontaneous and nonradiative recombination.
$S = |E(t)|^2$ is the photon number in the LD cavity. (output power P~S)
J is the carrier injection rate.

The feedback parameter is given by

$$\kappa = \frac{C_l}{\tau_0},$$

where parameter C_l which is a function of the facet and external mirror reflectivity R_2 and R_3

$$C_l = (1 - R_2)\sqrt{\frac{R_3}{R_2}}$$

is a measure of the coupling strength between the two cavities.

The relation between output power (P) and photon number (S) is discussed more in detail in the appendix A [6].

2.2 Steady-state analysis

Stationary lasing conditions can be obtained from (1), by setting E to be constant. The real and the imaginary parts of the equation ,when they are separated, can be written as

$$g - \frac{1}{\tau_p} = -2\kappa\cos\Omega\tau \tag{3}$$

$$\Omega_s - \Omega + \frac{\alpha}{2}\Delta g - \kappa\sin\Omega\tau = 0 \ . \tag{4}$$

In the absence of feedback, the threshold gain g_{th} is determined by

$$g_{th} = \frac{1}{\tau_p} \ . \tag{5}$$

Inserting (5) into (3) leads to a threshold gain shift

$$\Delta g(\Omega) = g - g_{th} = -2\kappa\cos\Omega\tau \ . \tag{6}$$

To find possible frequencies of lasing Ω_0 , insert (6) into (4) ; that gives

$$\Omega_s - \Omega = \kappa\alpha\cos\Omega\tau + \kappa\sin\Omega\tau \tag{7}$$

or

$$(\Omega_s - \Omega)\tau = \kappa\tau(\alpha\cos\Omega\tau + \sin\Omega\tau) = \kappa\tau\sqrt{1+\alpha^2}\,\sin(\Omega\tau + \theta)$$

$$(\Omega_s - \Omega)\tau = C\sin(\Omega\tau + \theta), \tag{8}$$

where

$$\theta = \arctan\alpha \tag{9}$$

and the feedback coefficient C is given by

$$C = \kappa\tau\sqrt{1+\alpha^2}\ . \tag{10}$$

The number of external-cavity modes is determined by the parameter C. For C<1 only one mode exists, while for C>1 there exists two or possibly more modes. For C>>1 the total number of modes is approximately given by $C/(\pi+1)$ (Fig.3 shows the solutions when increasing $\kappa\tau$). Furthermore for C>1, only half of the solutions, corresponding to $d\Omega/d\Omega_s > 0$ are stable with respect to slow fluctuations, representing, thus , possible frequency of stationary lasing. Ω_0 denotes the possible frequency of lasing. Inserting Ω_0 into Ω of equation (6) and (8), gives:

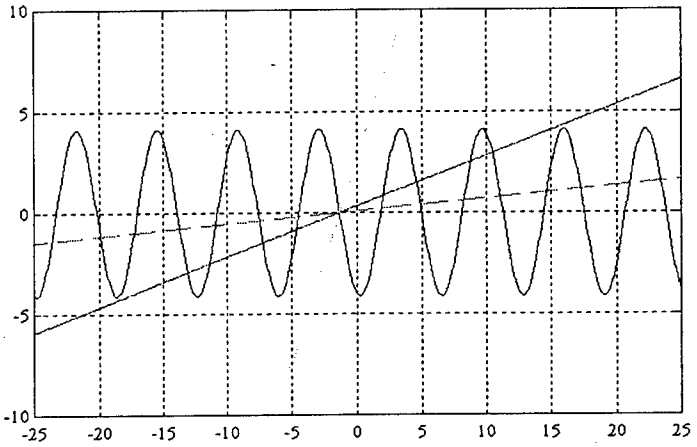

Fig. 3 The graphical representation of equation (11) for α=4. dashdot line for $\kappa\tau$=0.5 , solid line for $\kappa\tau$=4 and dash line for $\kappa\tau$=16 . intersection between the three lines and sinusoidal function is theoptical frequencyof the LD without EC.

$$\frac{\Omega_0 - \Omega_s}{\kappa} = -\sqrt{1+\alpha^2}\,\sin(\Omega_0\tau + \arctan\alpha) \tag{11}$$

$$\frac{\Delta g_{loss}}{2\kappa} = -\cos\Omega_0\tau\,. \tag{12}$$

The graphical representation of equation (11) is shown in Fig. 3. The solutions to equation (11) are the intersections between the line and the sinusoidal function [7]. Also when $\kappa\tau$<1 only one solution exists (the intersection between the dashdot line and the solution of the LHS of equation (11)) , increasing $\kappa\tau$ becomes more solutions (shown by the intersections between the other lines and the sinusoidal function) .

2.3 Compound-Cavity modes

Each lasing frequency Ω_0 has its own system of compound-cavity modes Ω_n. The lasing frequency Ω_0 and the compound cavity modes Ω_n should have the same

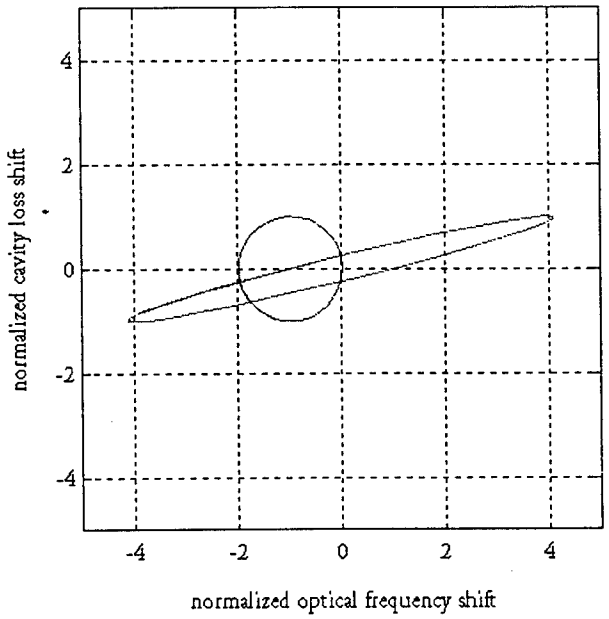

Fig.4 normalized cavity loss shift versus normalized optical frequency shift. the ellipse correspond to possible lasing frequency. The circle shows CC modes when the lasing frequency is equal to the optical frequency of the LD without EC.

Δg_{th}(threshold gain shift due to feedback). That gives

$$\Delta g_{th}(\Omega_n) = \Delta g_{th}(\Omega_0) = -2\kappa\cos\Omega_0\tau\,. \tag{13}$$

By inserting (13) and Ω_n into (7), we obtain

$$\Omega_s - \Omega_n = \kappa \sin \Omega_n \tau - \frac{\alpha}{2} \Delta g(\Omega_0) \,. \tag{14}$$

These compound-cavity modes Ω_n can be found by (14) times τ and subtracting the result from (11) times $\kappa\tau$, which yields

$$\frac{(\Omega_0 - \Omega_n)}{\kappa} = \sin \Omega_n \tau - \sin \phi_0 \,. \tag{15}$$

The graphical representation of (15) is shown in Fig . 5. The solutions to (15) are the intersections between the line and the sinusoidal function. As we can see in Fig. 5, increasing $\kappa\tau$ cause more and more solutions between the LHS and RHS of equation (15).

Let us consider the evolution of the CC modes with increasing $\kappa\tau$ in the plane of parameters normalized optical frequency shift $(\Omega_0 - \Omega_s)/\kappa$ -- normalized cavity loss shift $\Delta g_{loss}/2\kappa = -\cos\Omega_0 \tau$. In this plane, see Fig. 4 , all solutions of (8) belong to an ellipse [8]. For $\kappa\tau >> 1$ only those solutions of (11) that lie on the lower branch of the ellipse are unstable corresponding to $d\Omega_0 / d\Omega_s < 0$ [2].

The solutions of (15) lie on a circle with radius 1 in the same coordinates as Fig. 4. Equation (8) $\Delta\Omega\tau = \Omega\tau - \Omega_0\tau = -C\sin(\Omega\tau + \arctan\alpha)$ and a small-signal analysis yield the result for the linewidth of narrowing by external feedback [12]:

$$\Delta\nu = \Delta\nu_0 \left[1 + C\cos(\Omega\tau + \arctan\alpha)\right]^{-2} \tag{16}$$

where $\Delta\nu_0$ denotes the linewidth of the solitary laser diode.

The lowest spectral linewidth is obtained for $\phi_{ext} = \Omega\tau = -\arctan\alpha$, yielding

$$\Delta\nu = \frac{\Delta\nu_0}{(1+C)^2} = \frac{\Delta\nu_0}{(1+\kappa\tau\sqrt{1+\alpha^2})^2} \,. \tag{17}$$

The mode with the lowest threshold gain to start lasing is $\Delta g_{th} = -2\kappa\cos\Omega\tau = -2\kappa$ when $\cos\Omega\tau = 1$ and thus

$$\Delta\nu = \frac{\Delta\nu_0}{(1+\kappa\tau)^2} \quad \text{for } \phi_{ext} = 2\pi m \,, \quad m = 0,1,2,\cdots\cdots \,. \tag{18}$$

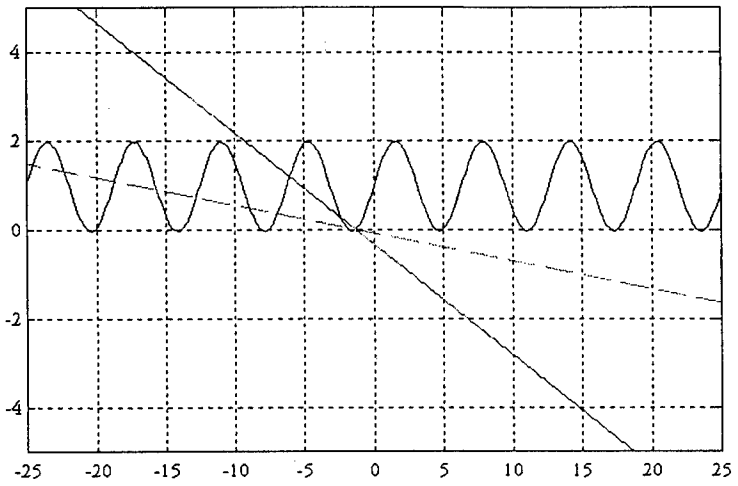

Fig.5 The graphical representation of equation (15). Dash-dotted line for $\kappa\tau$=0.5, solid line for $\kappa\tau$=4 and dash line for $\kappa\tau$=16.

One would more expect that the mode with the lowest threshold gain would be the lasing one. Surprisingly, it turns out that the measured spectral linewidth for laser diode with optical feedback coefficients C>>1 is closer to equation (16) than to (18), indicating that the external cavity mode with the narrowest linewidth is more stable than the external cavity mode with the lowest threshold gain.

From the measured conclusion, we assume $\Omega_0\tau = -\arctan\alpha$ corresponds to laser oscillation with minimal linewidth. In Fig. 4 the circle is shown for the case of $\Omega_0 = \Omega_s$. It means that the lasing frequency Ω_0 is equal to the resonance optical frequency Ω_s of the LD without EC. The intersections between the ellipse and the circle are four points. One of the points marked A in Fig. 4 is when $\Omega_0 = \Omega_s$ and its coordinates are $\left[(\Omega_0 - \Omega_s)/\kappa, -\cos\phi_0\right]$. Another point B has coordinates , $\left[(\Omega_1 - \Omega_s)/\kappa, -\cos\phi_0\right]$ where

$$\Omega_1 = \Omega_0 + 2\kappa\sin\phi_0 \quad . \tag{19}$$

The points A and B have the same optical loss $\Delta g_{loss} = -2\kappa\cos\Omega_0\tau$ as the lasing mode Ω_0 , they can be oscillating modes at the same time.

For $\kappa\tau < 1$ (weak feedback), $\Omega_0 = \Omega_n$ is the only solution to equation (15). And it cannot be the lasing one because the optical loss is higher than the lasing one (point A). Increasing $\kappa\tau$, it leads to equalization of the cavity losses for the main mode (point A) and the sidemode when the last one reaches point B. Point B (the sidemode) has the same optical loss as point A (the main mode) and could be the lasing one too. However point B is lying on the upper unstable

branch of the ellipse, so it cannot be the lasing one for the solitary LD without EC. For the LD with EC, reaching point B by the CC sidemode can be considered as the transition from stable CW operation at frequency Ω_0 to instability. The critical value of $\kappa\tau$ to reach point B can be found by the following steps. From the x-axis of Fig. 4 at point B,

$$\cos\Omega_1\tau = \cos\phi_0 \equiv \cos\Omega_0\tau \quad . \tag{20}$$

Ω_1 also meets one of the solutions of equation (15). By inserting Ω_1 into Ω_n of equation (15), we get

$$(\Omega_0 - \Omega_1)\tau = \kappa\tau(sin\Omega_1\tau - \sin\phi_0) \tag{21}$$

Inserting equation (19) $\Omega_1 = \Omega_0 + 2\kappa\sin\phi_0$ into Ω_1 on the LHS of equation (21) yield

$$\sin\Omega_1\tau = -\sin\phi_0 \quad . \tag{22}$$

From equations (21) and (22), we have

$$\Omega_1\tau = \Omega_0\tau - 2\pi - 2\phi_0 \; . \tag{23}$$

After multiplying equation (18) by τ and subtracting (22) into it, one obtains the "steady-state" condition of instability of the form

$$\kappa\tau = \frac{\pi + \phi_0}{-\sin\phi_0} \; . \tag{24}$$

Equation (24) also satisfies equation (11).

Equation (24) defines the critical value of feedback under two conditions: $\phi_s = -\arctan\alpha$ and $\Omega_0 = \Omega_s$. We could associate each state of lasing with its own number N. The point A, one of lasing state nearest Ω_s is set to be N=0. We denote ${\Omega_0}^N$, the lasing frequency for the Nth state, and ${\phi_0}^N$, the detuning parameter for the Nth state. Then we can find the next relation for the phase shift

$${\Omega_0}^N = \Omega_s\tau - 2\pi N - \phi_s + {\phi_0}^N \qquad N = 0, \pm1, \pm2, \cdots\cdots \; . \tag{25}$$

ϕ is the detuning parameter between $(-\pi, \pi)$, and $\Omega_i\tau = 2\pi n + \phi_i$.

Combining (24) and (25) in (7), we obtain

$$\tan \phi_0^{\,N} = -\frac{\alpha(\pi + \phi_0^{\,N})}{\pi(2N+1) + \phi_s} \quad . \tag{26}$$

This is the equation for the critical value of phase detuning .

To find the critical feedback coefficient value to reach the "steady-state" condition (24) of instability for each state of lasing, we combine

$$\kappa\tau = \frac{1-R}{\sqrt{R}} \cdot \frac{\tau}{\tau_0} \cdot \sqrt{f_{ext}}$$

for Fabry-Perot laser and (23). That gives

$$\kappa\tau = \frac{1-R}{\sqrt{R}} \cdot \frac{\tau}{\tau_0} \cdot \sqrt{f_{ext}^{\,N}} = \frac{\pi + \phi_0^{\,N}}{-\sin \phi_0^{\,N}}$$

then,

$$f_{ext}^{\,N} = \frac{R}{(1-R)^2} \cdot \frac{(\pi + \phi_0^{\,N})^2}{\sin^2 \phi_0^{\,N}} \cdot \left(\frac{\tau_0}{\tau}\right)^2 \quad . \tag{27}$$

The relation between main mode and sidemode (CC mode) of the Nth lasing state can be found by using equation (23) ,

$$\Omega_1^{\,N} \tau = \Omega_0^{\,N} \tau - 2\pi - 2\phi_0^{\,N} \ ,$$

i.e.,

$$\Omega_1^{\,N} = \Omega_0^{\,N} - 2\pi(1 + \frac{\phi_0^{\,N}}{\pi}) \cdot \frac{1}{\tau} \quad .$$

Then,

$$\Omega_1^{\,N} = \Omega_0^{\,N} - 2\pi\nu_N \tag{28}$$

where

$$\nu_N = \left(1 + \frac{\phi_0^{\,N}}{\pi}\right) \cdot \frac{1}{\tau} \tag{29}$$

can be interpreted as the beating frequency between two CC modes having equal optical loss.

In equation (24) $\kappa\tau$ should be greater than zero, so ϕ_0 has values between $(-\pi, 0)$. That is, the detuning parameter is negative. This condition translates to

$$1 + \frac{\phi_0^{\,N}}{\pi} < 1$$

which gives

$$\nu_N < \frac{1}{\tau}, \tag{30}$$

from equation (29). So the mode beating frequency is always less than EC-mode spacing $1/\tau$.

The steady-state analysis of the short EC LD will help us to find the critical value of the feedback parameter leading to possible instabilities in laser operation. Now, we will prove the instability of laser operation by using the dynamic analysis including the linear stability analysis and computer simulation.

2.4 Linear Stability analysis

The static solution is called stable, if small perturbations from the static solution decay to zero as time goes toward infinity. Such a stable static solution can be observed experimentally. To check the stability of the static solution, we perform the linear stability analysis for a given static solution. Let $\delta E, \delta\phi$,and δN denote the deviation from the stationary solution . The criterion for stable operation is that the determinant D(s) has no zeros in the right half of the S-plane [7], [9]. The determinant is obtained as

$$\begin{aligned} D(s) = & -s^3 + s^2\left[\gamma + 2\kappa e(\tau)\cos\phi\right] \\ & -s\left[{\omega_R}^2 + \kappa^2 e^2(\tau) + 2\gamma_e \kappa e(\tau)\cos\phi\right] \\ & +\kappa\left[{\omega_R}^2 e(\tau)(\cos\phi - \alpha\sin\phi) + \gamma_e \kappa e^2(\tau) + \alpha\gamma_e\gamma_p e(\tau)\sin\phi\right] \end{aligned} \tag{31}$$

with $e(\tau) = 1 - e^{i\omega\tau}$ and $\phi = \Omega\tau$. Here $\gamma_e = 1/\tau_s + g_N S$ is the carrier perturbation decay rate, $\gamma = \gamma_e + \gamma_p$ is the decay rate of relaxation oscillations, with $\gamma_p = g\kappa_p P$ being the contribution of the nonlinear gain. The angular frequency of relaxation oscillations ω_R is given by ${\omega_R}^2 = g g_N S + \gamma_e\gamma_p$. Assuming that

$${\omega_R}^2 >> \gamma_e\gamma_p \quad , \quad {\omega_R}^2 >> \kappa\gamma_e$$

then D(S) can be approximated by

$$\begin{aligned} D(s) = & -s^3 + s^2\left[\gamma + 2\kappa e(\tau)\cos\phi\right] \\ & -s\left[{\omega_R}^2 + \kappa^2 e^2(\tau)\right] \\ & +\kappa\left[{\omega_R}^2 e(\tau)(\cos\phi - \alpha\sin\phi)\right] \end{aligned} \tag{32}$$

For $s = j\omega$, we can separate the equation (32) into the real and imaginary parts. The real part of the equation is related to the damping constant of the semiconductor laser rate equations, and the imaginary part is related to the small signal resonance frequency.

The real and the imaginary parts give the following two conditions for having stable solutions located in the left half of the complex S plane (The detail is shown in Appendix B) :

$$(1-2\frac{\omega^2}{{\omega_R}^2})\cos\phi_0 - \alpha\sin\phi_0 < 2\frac{\kappa\omega}{{\omega_R}^2}\sin\omega\tau + \frac{\omega^2}{\kappa{\omega_d}^2}\frac{1}{1-\cos\omega\tau} \tag{33}$$

$$\omega^2 - {\omega_R}^2 = 4\kappa^2\sin^2(\frac{\omega\tau}{2}) + \omega\gamma\cot(\frac{\omega\tau}{2}) \tag{34}$$

where $\omega_d = {\omega_R}^2/\gamma$ is the damping frequency of the relaxation oscillations of LD without EC, $\phi_0 = [\Omega_0\tau] \bmod (2\pi)$ is the optical phase shift in EC, or detuning parameter.

If we neglect the first term on the right hand side (RHS) of the equations (33) and (34), the remaining terms $1/{\omega_d}^2$ and γ describe the relaxation oscillation - induced instability which causes coherence collapse for long EC LD and very weak feedback. The first terms in the RHS of equation (33) and (34), which are proportional to κ^2 and κ, respectively, are thus of important in the case of sufficiently high levels of feedback and reflect the influence of the above-described CC-mode competition on stability of the short EC LD.

In the case of sufficiently high levels of feedback, we neglect the second term on the RHS of both (33) and (34) and assume $2\omega^2/{\omega_R}^2 >> 1, \alpha$. We then obtain from (33) and (34) ,

$$\cos\phi_0 = -\frac{\kappa}{\omega}\sin\omega\tau \tag{35}$$

$$\omega = 2\kappa\sin(\frac{\omega\tau}{2}) \tag{36}$$

When the frequency of self-oscillations $\omega/2\pi$ is equal to the CC-mode beat frequency from equation (19), we get

$$\frac{\omega}{2\pi} = \nu_n = (1+\frac{{\phi_0}^N}{\pi})\cdot\frac{1}{\tau} \tag{37}$$

which yields

$$\omega\tau = 2\pi + 2{\phi_0}^N \tag{38}$$

By inserting (38) into (35) or (36) ,we can get the same expressions as (14) :

$$\kappa\tau = \frac{\pi + \phi_0}{-\sin\phi_0}$$

Thus, the linear stability analysis of the short EC LD not only gives the critical value of κ but also predicts the dynamic instability of laser operation caused by the competition of the two CC modes which have equal optical losses.

Equations (31) and (32) give the boundary of this stability region. But they cannot give any information above the stability boundary. To get the information above the boundary of the stability region, we proceed to use computer simulations of the nonlinear system.

3.0 Numerical Simulation

The rate equations for the EC LD are given in equations (1) and (2). The absolute squared value of the electric field amplitude corresponds to the number of photons in the laser cavity. Equations (1) and (2) can be cast into rate equations for the photon number S, the phase ϕ , and the carrier number N.

$$\frac{dS(t)}{dt} = (g - \frac{1}{\tau_p})S(t) + 2\kappa\sqrt{S(t)}\sqrt{S(t-\tau)}\cos(\Omega_s\tau + \phi(t) - \phi(t-\tau)) \quad (39)$$

$$\frac{d\phi(t)}{dt} = \frac{\alpha}{2}g_N(N - N_s) - \kappa\frac{\sqrt{S(t-\tau)}}{\sqrt{S(t)}}\sin(\Omega_s\tau + \phi(t) - \phi(t-\tau)) \quad (40)$$

$$\frac{dN(t)}{dt} = J - \frac{N(t)}{\tau_{sp}} - gS(t) \quad (41)$$

In numerical simulations, the system of rate equations system (39)-(40) is solved by using a fifth-order Runge-Kutta method [10],[11]. The calculations used the laser parameters given in Table I .The computer program is written in C (shown in Appendix C). We specify the initial conditions S(0)=10, $\phi(0)=0$ and N(0)=0. In the time interval $0 \le t \le \tau$, the data of photon number S and phase ϕ are stored in memory and they are reused after the round-trip time τ of the EC in order to account for the optical feedback.

Next, we will show results for the two different kinds of SEC LD: A) Fabry-Perot laser with an external cavity; B) VCSEL with an external cavity

3.1 Fabry-Perot Laser with an external cavity

The first example is a Fabry-Perot laser with an external cavity as shown in Fig.2, with cavity length L=200um, facet reflectivity R=0.32 (corresponding to KL=2.3 for an AR-coated

DFB laser with a $\pi/2$ phase shift.), output power P=5mW/per facet. Other parameters are given in Table I [12]. We choose EC cavity length such that round-trip time τ varies between 25 and 40 ps (the external cavity between 3.75 and 6 mm). Within this range, τ is less than the critical value for coherence-collapse regime (chaotic self-modulation of laser light with dramatic broadening of laser spectrum).

TABLE I
List of Parameters for Fabry-Perot laser

Parameter	Symbol	Value	Units
scattering loss in the active region	α_s	3.6×10^{3}	m^{-1}
carrier number at transparency	N_s	2.0×10^{8}	
output power	P	$2.906\times10^{-8}\times S$	*mW / facet*
index of active region	n_g	4.5	
differential gain	g_N	2.2×10^{3}	s^{-1}
linewidth enhancement factor	α	4	
laser wavelength	λ	1.3	*um*
spontaneous emission lifetime	τ_s	2.0×10^{-9}	*s*
photon lifetime	τ_p	1.29072×10^{-12}	*s*
gain saturation coefficient	k_p	4.8	W^{-1}

Figs. 6 and 7 illustrate two characteristics of SEC LD instability. In Fig. 6 we report the simulated and analytical dependence of the oscillation according to the feedback parameter (f_{ext}) on the length of external cavity (Lext). The dependence of the frequency of these oscillations on the length of external cavity (Lext) is shown in Fig. 7 . The two dash lines in Fig. 6 and Fig. 7 represent two groups of strongest high-frequency oscillations (the modulation depth reaches unity) according to numerical simulation. Data marked with asterisks are the simulation data of high frequency oscillations. The lower dash line belongs to the first group of high frequency oscillation according to $f_{ext}^{\ 0}$ .The second dash line belongs to the second group of high frequency oscillation according to $f_{ext}^{\ 1}$.

As discussed the results in Fig. 6 and Fig. 7 are obtained under two assumptions. First, $\phi_{ext} = -\arctan\alpha$, the lowest spectral linewidth, is more stable than the lowest threshold gain as mentioned before. Second, $\Omega_0 = \Omega_s$ means the lasing frequency Ω_0 is equal to Ω_s , the resonance optical frequency of the LD without EC . We can see from the high feedback parameter (f_{ext}) that the laser operation will lose stability and lead to high frequency oscillation.

This type of instability is the result of the beat frequency between two CC modes having equal optical loss. As mentioned in the previous section, by increasing f_{ext} it leads to equalization of the cavity losses for the main mode and the first left sidemode and those two

modes produces a self twin-mode locking generating high frequency oscillations. In. Fig 6 the two solid lines present the critical feedback parameters from equation (27) (the lower solid line shows N=0 for f_{ext}^{N} and the other shows N=1), corresponding to the main mode and the sidemode having equal optical loss. The two solid lines as shown in Fig.7 illustrate the results from equation (29) (the lower solid line shows N=0 for ν_N and the other shows N=1). These results denote the beat frequencies between two CC modes having equal optical loss. From Fig. 6 and Fig. 7 linear stability analysis and computer simulated agree very well.

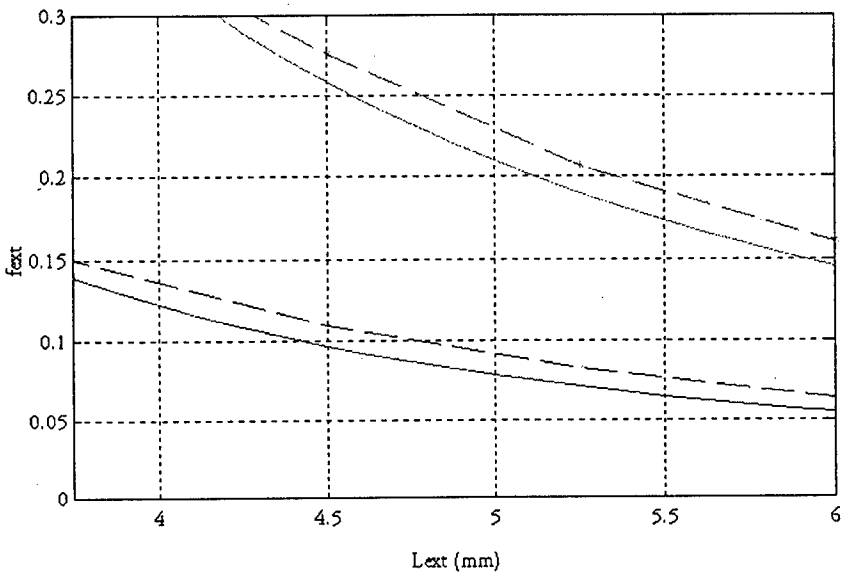

Fig. 6 A SEC LD operation (Lext,fext). The lower and upper solid lines present theoretical critical value at f_{ext}^{0} and f_{ext}^{1} group . The lower and upper dash lines show the strongest oscillation at f_{ext}^{0} and f_{ext}^{1} group. Curved marked with '*' represent the simulation data..

In what follows, we explain the data within the onset and offset of high frequency oscillations of the group f_{ext}^{1} for an air-equivalent EC length Lext=5.25mm (τ=35 ps). For f_{ext} =0.204 the high frequency oscillation occurs at a frequency around 20.9 GHz. But the oscillation is not strong, the amplitude of the oscillation will become weaker and it will disappear after t>52ns. Increasing f_{ext} to 0.205 the stable oscillation occurs. But the amplitude of the oscillation is small. That means the intensity of the sidemode is much less than the main mode. Further increase in f_{ext} leads larger oscillation amplitude (the stronger intensity of the sidemode) and the bigger oscillation frequency. When f_{ext} reaches 0.206 the strongest intensity shows up as shown in Fig. 8 with the frequency f=21.3 GHz. Further increase in f_{ext} (>0.206) destroys the twin-mode locking. It leads the high frequency oscillation to a new single-mode state with higher output power (6.56 mW). The new optical frequency does not the same with any of the "old" CC

modes in Fig. 8 . The new one is one of the stable solutions (which lie on the lower branch of Fig. 4) of equation (8).

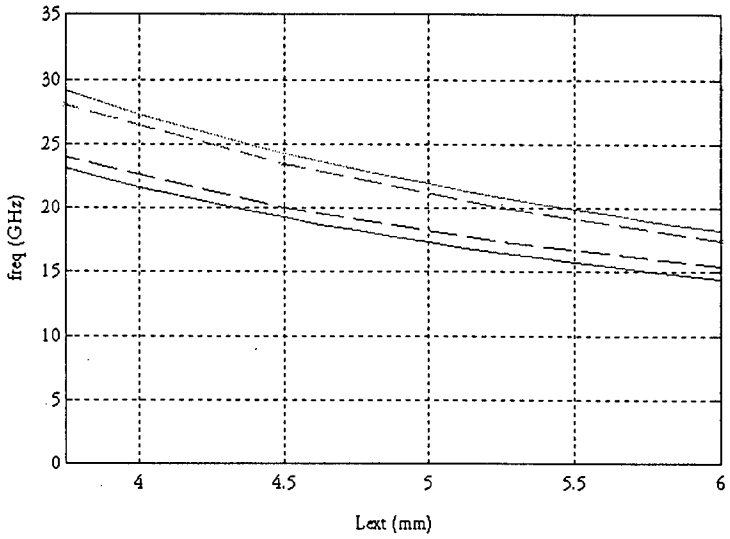

Fig. 7 A SEC LD operation (Lext,f). The lower and upper solid lines present the theoretical critical value at f_{ext}^{0} and f_{ext}^{1} group . The lower and upper dash lines show the beat frequencies of the f_{ext}^{0} and f_{ext}^{1} according to the strongest oscillation in Fig. 11. Curved marked with '*' represent the simulation data.

From the theoretical and simulated results, we conclude that: for the high feedback parameter f_{ext}, increasing f_{ext} causes the single-mode optical frequency to become unstable above a critical f_{ext}. It leads to high-frequency oscillation corresponding to self twin-mode locking. Increasing f_{ext} destroys mode locking. If feedback f_{ext} is further increased, above process will repeat.

Thus, we can see that a SEC LD exhibits several regimes of self twin-mode locking high frequency oscillations in some ranges of feedback parameters.

The simulation we have done corresponds to an output power P=5mw/per facet. It agree with the results in [4]. The critical feedback parameters required for high frequency oscillation also change with the change of the injection number according to the simulated results.

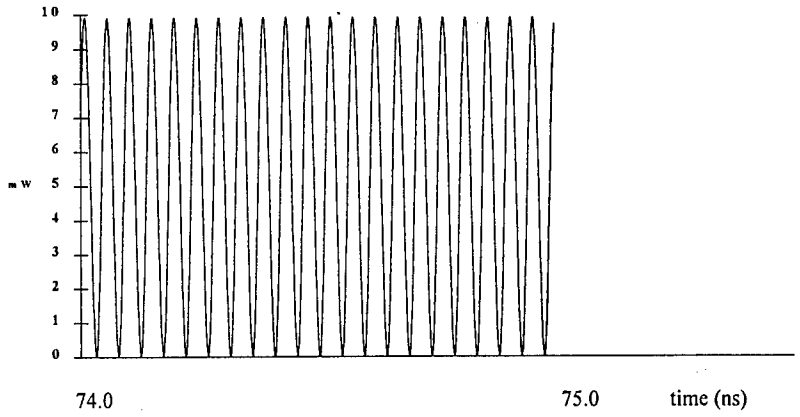

Fig. 8 The strongest oscillation for the Lext=5.25mm and the f_{ext}^{1} group. The feedback parameter is 0.206. The oscillation frequency is equal to 21.3 GHz.

In what follows, we set the output power P=2 mW/per facet. Other parameters are the same as the previous example as shown in Table I. Here, we also choose the EC length L_{ext} =5.25 mm. We found that the feedback parameters for the strongest modulation index occurs when f_{ext} = 0.188 compared to 0.206 for P=5 mW/per facet. Further increasing f_{ext} destroys the twin mode locking. It leads the laser operation on a new single-mode state with higher output power (3.06 mW). The strongest oscillation frequency we get in the group f_{ext}^{1} is 20.7 GHz. This frequency is not the same with the frequency 21.3 GHz in the previous example of P=5 mW/per facet.

Table II
List of frequency, average power and oscillation amplitude on the change of the injection current

Injection current (mA)	frequency (GHz)	Average Power (mW)	Osc. Amp. (mW)
47.87	0	6.279	0
48.23	21.3	4.925	4.775
48.39	21.2	4.95	4.95
48.55	21.1	5.06	4.89
48.71	21.05	5.05	4.55
48.84	21.03	5.12	4.0
48.85	21.02	5.123	3.925
48.865	21.01	5.125	3.825
48.87	21	5.163	0.123
49.03	20.9	5.228	0.007
49.19	20.7	5.2875	0.0005

Next, we will show the dependence of the oscillation frequency (f), average power (P) and oscillation amplitude on the injection current (I=J/e). The external cavity length is fixed at Lext=5.25 mm and the feedback parameter is fixed at f_{ext}=0.206. The other parameters are shown in Table I. In Table II and Fig. 9 (a),(b),(c) , we can see the lead to higher oscillation frequency variations of these quantities for injection current values between 48.2 mA and 49.2 mA. The laser operation of f_{ext}=0.206 and injection current I=47.87 mA destroys the twin-mode locking and leads to a new single-mode state with higher output power 6.279 mW. For I>48.23mA the high frequency oscillation occurs. The strongest oscillation shows up when I=48.39 mA at a frequency 21.2 GHz . Further increasing injection current I leads the weaker oscillation. When I>49.19mA, the stable oscillation disappears. Thus, the injection current are functions of the oscillation frequency, the oscillation amplitude and the average output power

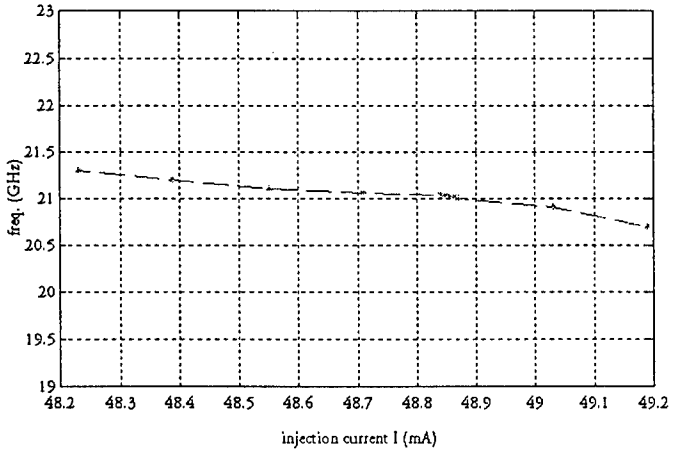

(a)

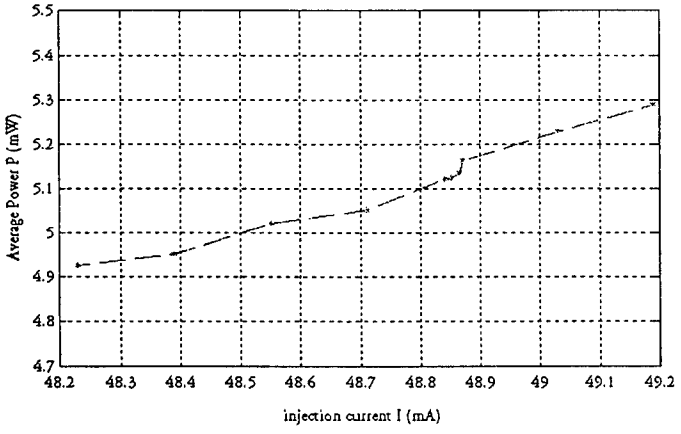

(b)

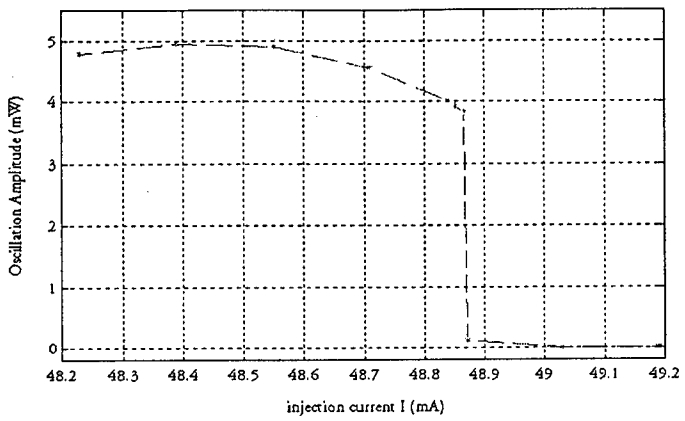

(c)

Fig. 9 The parameters of the laser operation depend on the injection current (I) at an external cavity length Lext=5.25 mm and the feedback parameter f_{ext}=0.206 . Data asterisks are the simulation data.(a) Oscillation frequency versus the injection current (I). (b) Average output power versus the injection current (I). (c) Oscillation Amplitude versus the injection current (I).

According to the simulated results, the SEC LD operation do exist some instability regimes. The feedback parameters of the onset and offset of the instability depends on the output power. The oscillation frequencies also depends on the output power. But the theoretical critical feedback value in equation (27) cannot show any information about the relation between f_{ext} and Power. The theoretial frequency value in equation (28) also cannot give any information about the relation between frequency and Power. Those should be investigated in more detail.

An interesting question is: what is the highest oscillation frequency? By inserting $\kappa = C_l / \tau_0$ into equation (24) and equation (24) $\pi + \phi_0 = -k\tau \sin\phi_0$ into equation (29), we get

$$\nu = [-\sin\phi_0]\frac{C_l}{\pi}\cdot\frac{1}{\tau_0} \tag{42}$$

where

$$C_l = (1-R_2)\cdot\sqrt{\frac{R_3}{R_2}} = (1-R_2)\cdot\sqrt{\frac{f_{ext}}{R_2}}$$

is a coupling strength coefficient between the EC and the LD. From equation (42) , we can see that higher f_{ext} and shorter LD (means shorter τ_0) lead to higher oscillation frequency.

To obtain the highest oscillation frequency, we also need to set $-\sin\phi_0 = 1$ in equation (42). Then we get

$$\nu_{\max} = \frac{1}{\pi\tau_0},$$

assuming η=1. Thus, the highest frequency is equal to the mode spacing, $\nu = 1/\tau_0 = c/2Ln_g$, for the LD without the EC.

Whether this high frequency limit can really be achieved and where the stability of the high frequency regimes really are still need to be investigated in more detail.

3.2 VCSEL with an External Cavity

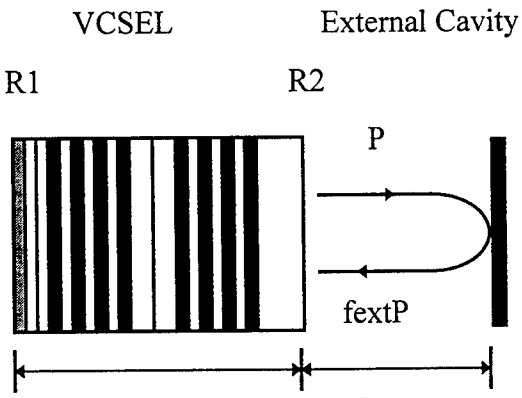

The system is schematically represented in Fig.10 , where R1=0.999 (for the top mirror), R2=0.995 (for the bo Schematic of a VCSEL cavity with an external cavity im. The other parameters used in the following simulation are shown in Table III .

According to our simulation, the result of simulation agrees with analysis only when the average output power of VCSEL is around 15.7 mW *. This power is too high for the VCSEL opearion. Hence we will show the simulated results corresponding to the output power P=2mW/the bottom facet. In Fig.11, we show the locations of strongest high frequency oscillations in the parameter space consisting of the feedback parameter (f_{ext}) and the length of external cavity (Lext). The graphical representation of the high frequency oscillations (f) as a function of the length of the external cavity (Lext) is shown in Fig.12. As before, the dash lines are fits to simulated results marked with asterisks.

TABLE III
List of Parameters for VCSEL

Parameter	Symbol	Value	Units
scattering loss in the active region	α_s	3.6×10^3	m^{-1}
carrier number at transparency	N_s	1.41372×10^9	

output power	P	$2.653\times10^{-8}\times S$	mW / the bottom facet
index of active region	n_g	3.5	
diameter of VCSEL's	r	15	um
differential gain	g_N	2.2×10^{3}	s^{-1}
linewidth enhancement factor	α	4	
laser wavelength	λ	966	nm
spontaneous emission lifetime	τ_s	2.0×10^{-9}	s
photon lifetime	τ_p	1.766×10^{-12}	s
gain saturation coefficient	k_p	4.8	W^{-1}

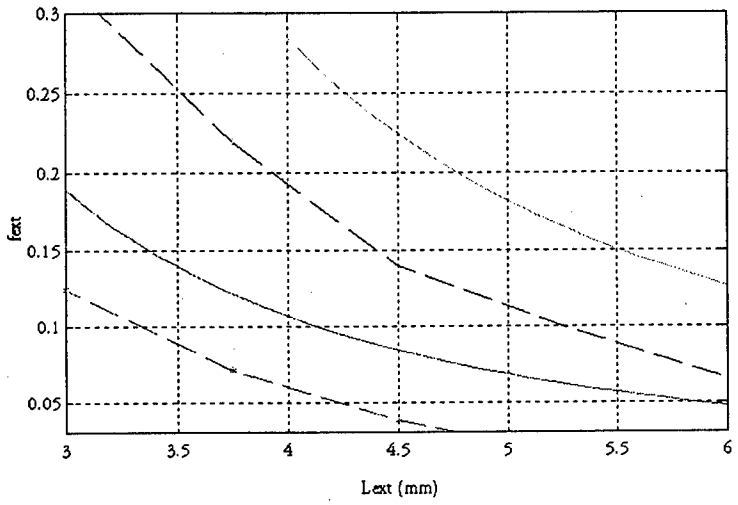

Fig. 11 A VCSEL with a SEC operation (Lext ,fext). The lower and upper solid lines show the critical value at $f_{ext}^{\ 0}$ and $f_{ext}^{\ 1}$ group. The lower and upper dash lines show the strongest oscillation at and $f_{ext}^{\ 1}$ group Curved marked with '*' represnet the simulated data. The parameters for the strongest oscillation at an average output power around 15.7mW ,coincide with the critical parameters for the onset of oscillation according to analysis. The range of parameters for oscillations is relatively small.

As we can see, shorter laser cavity length as for the case of a VCSEL also lend to twin-mode locking and high frequency oscillations. The lower dash line in Fig.11 and Fig.12 show the strongest oscillation just before switching to a new single-mode state for $f_{ext}^{\ 0}$ and the upper ones for $f_{ext}^{\ 1}$. Increasing f_{ext} causes the instability to switch to a new single-mode state. This process repeats if f_{ext} continues to increase (for $f_{ext}^{\ N}$, N=0,1,2,3 .....) .

Next, we will explain the instability regime of VCSEL operation for an external cavity length Lext = 3.75 mm (the instability group for f_{ext}^{0} only). The onset of instability is f_{ext}=0.07 with the weak intensity of sidemode. Increasing f_{ext} results in stronger intensity of sidemode thus stronger oscillation. When f_{ext} reaches 0.071 as show in Fig.13 the modulation depth reaches unity (the strongest oscillation) with a frequency of 18ghz. Increasing f_{ext} further destroys the twin-mode locking instability and lead to a higher power (~4.496mW) in a single-mode state. These changing in the strength of the oscillation repeat for f_{ext}^{N} , N=0,1,2,3 ..... .

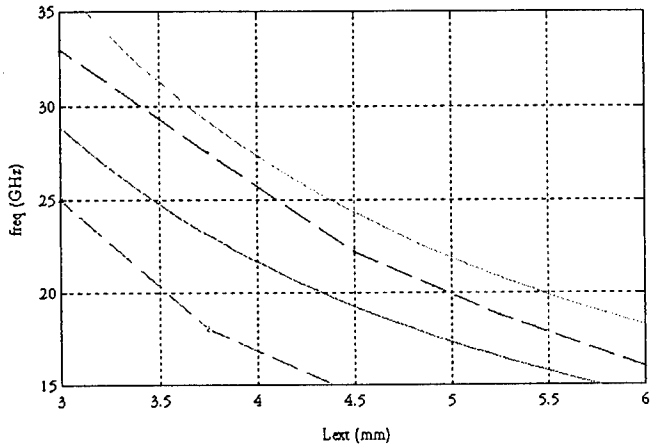

Fig. 12 A VCSEL with a SEC operation (Lext ,f). The lower and upper solid lines show the critical beat frequencies of the f_{ext}^{0} and f_{ext}^{1} group. The lower and upper dash lines show the beat frequencies of the and f_{ext}^{1} group according to the strongest oscillation in Fig.11. Curved marked with '*' represent the simulated data.

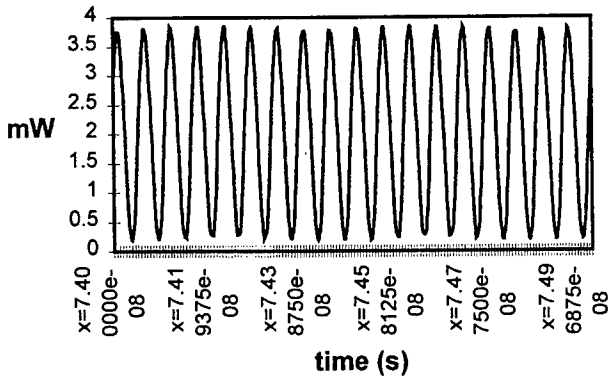

Fig. 13 The strongest oscillation in Lext=3.75mm and the f_{ext}^{0} group. The feedback parameter is 0.071. The oscillation frequency is 18 GHz.

Next, we will show the dependences of the oscillation frequency (f), average power (P) and oscillation amplitude on the injection current (I=J/e). The external cavity length is fixed at Lext=3.75mm and the feedback parameter is fixed at f_{ext}=0.071. The other parameters are shown in Table III. In Table IV and Fig.14 (a),(b),(c) , we can see the variations of these quantities for injection current values between 138.8mA and 193.8mA. The laser operation for f_{ext}=0.071 and injection current I=138.83mA detroys the twin-mode locking and leads to a new single-mode state with higher output power 4.329mW. For I>138.99mA the high frequency oscillation occurs. The strongest oscillation shows up when I=139.07mA at a frequency 18 GHz. Further increasing

Table IV

List of frequency, average power and oscillation amplitude on the change of the injection current.

Injection current (mA)	frequency (GHz)	Average Power (mW)	Oscillation Amplitude (mW)
138.83	0	4.329	0
138.99	18.1	2.0	1.80
139.07	18.0	2.025	1.825
139.15	18.0	2.045	1.7
139.23	18.0	2.085	1.55
139.31	18.0	2.125	0.105
139.47	17.9	2.199	0.016
139.63	17.8	2.276	0.001

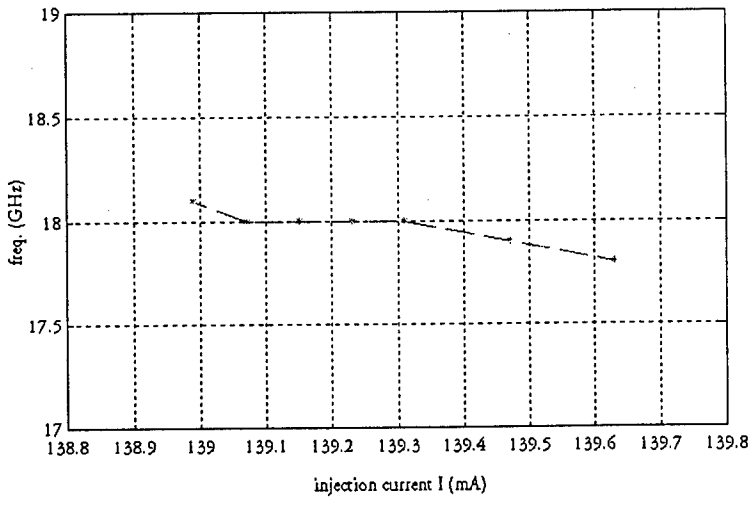

(a)

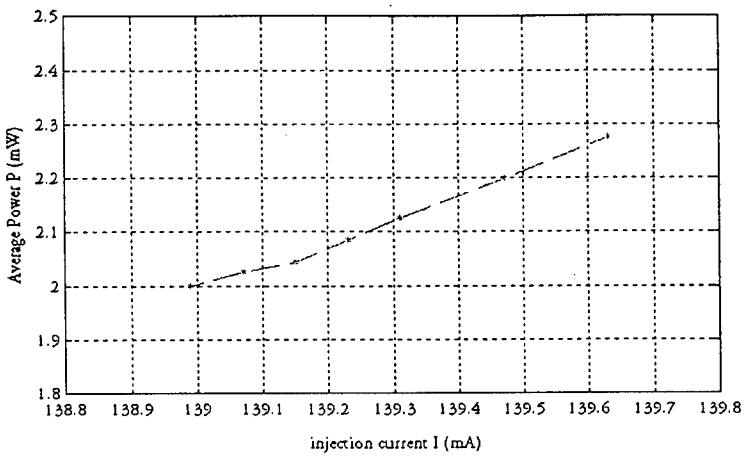

(b)

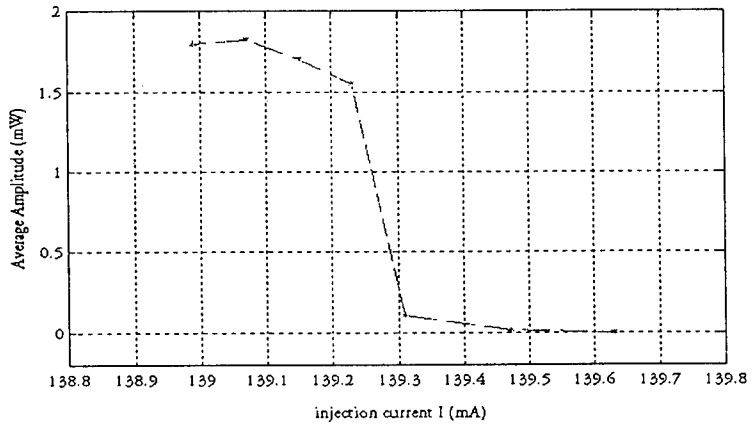

(c)

Fig.14 The parameters of the laser operation depend on the injection current (I) at an external cavity length Lext=3.75mm and the feedback parameter f_{ext}=0.071 . Data marked asterisks are the simulation data. (a) Oscillation frequency versus the injection current (I). (b) Average output power versus the injection current (I). (c) Oscillation Amplitude the injection current.

injection current I leads the weaker oscillation. When I>139.63mA, the stable oscillation disappears.

Due to the simulated results in Fabry-Perot lasers and VCSEL, we can conclude that: the SEC LD exhibits some regimes of high-frequency self-oscillations in some range of feedback parameters. For fixed Lext and f_{ext} , the change of the injection current will cause the change of the oscillation frequency, the oscillation amplitude and the average output power.

4.0 Conclusion

We have presented analytical and numerical investigation of the instability regimes of a SEC LD . The instability is caused by self twin-mode locking of a short external cavity (a few millimeters) laser diode. As we have proved theoretically, these high-frequency oscillations correspond to an equalization of the cavity loss for the main mode (the lasing frequency) and the sidemode. The phenomena of high-frequency oscillation is caused by a high level of coupling between the laser diode and the external cavity and thus are compound-laser-cavity effects.

The key results are as follows: First, a laser diode operation with a short external cavity (a few millimeters) in some ranges of feedback parameters exist some regimes of high-frequency self twin-mode oscillations. Second, in high frequency oscillation of every f_{ext}^{N} (N=0,1,2.....) regime, increasing f_{ext} leads to higher modulation index and higher oscillation frequency. For certain f_{ext} the strongest oscillation amplitude shows up (the modulation depth reaches unity). Increasing f_{ext} destroys the twin-mode locking instability and lead to a higher power single-mode state. These instability repeat for every f_{ext}^{N} regime.

In the simulation results, changing injection number (J) (or injection current (I)) will change the average output power. In addition to changing the output power, it also changes the critical feedback parameter f_{ext} which required for high-frequency oscillations and the oscillation frequency. But in equations (26) and (29), the critical feedback parameters and the beat frequencies do not depend on either the injection number or the output power. The validity of these questions should be investigated further.

In numerical simulation, we used two kinds of laser cavities, Fabry-Perot laser and VCSEL. The numerical and analytical results demonstrate that a SEC LD operation do exhibit high-frequency self twin-mode locking oscillations in some ranges of feedback parameters. These should be proved by experiments.

This laser operation of a SEC LD can be used as tunable microwave oscillators with frequency modulation capacities. These device can be very useful for all-optical high-speed microwave fiber-optic transmitters.

Appendix A

To find the relation between output power (P) and photon numbers (S), we should discuss the two main sources of loss in optical resonators first. The two most common loss mechanisms in an optical resonator are as follows:

1. Losses resulting from absorption and scattering in the laser medium between the mirrors. α_s is the absorption coefficient of the medium corresponds to photons which are lost within the laser cavity.
2. Losses arising from nonperfect reflections at the mirrors. Reflection loss is unavoidable, since without some transmission no power output is possible. Even we design the mirrors with the highest possible reflectivities, some residual absorption and scattering reduce the reflectivity to somewhat less than 100 percent.
3.

The threshold gain denoted $g = g_{th}$, equals to an effective overall distributed-loss coefficient,

$$g_{th} = \alpha_s + \alpha_m , \tag{A-1}$$

where the quantity

$$\alpha_m = \frac{1}{2L} \cdot \ln(\frac{1}{R_1 R_2}) \tag{A-2}$$

represents a fictitious equivalent loss per unit length due to useful escape of light through one of the two cavity mirrors. The reflectances of the two mirrors are R1 and R2.

The external quantum efficiency of the LD, η_{ext}, is the fraction of injected electrons that get converted to useful output photons. The quantity η_i is the internal quantum efficiency, the fraction of injected electrons that produce stimulated photons, not all of which will reach the output of the LD. The ratio between the external and the internal quantum efficiency is given as

$$\frac{\eta_{ext}}{\eta_i} = \frac{\alpha_m}{g_{th}} = \frac{(\frac{1}{2L}) \cdot \ln(\frac{1}{R_1 R_2})}{g_{th}} = \frac{\alpha_m}{\alpha_s + \alpha_m} \tag{A-3}$$

Therefore, total emitted power P_{tot} due to stimulated emission is

$$P_{tot} = (h\nu) \cdot \frac{\eta_{ext}}{\eta_i} \cdot (\text{\# of photons due to stimulated emission per unit time}) \tag{A-4}$$

that is,

$$P_{tot} = (h\nu) \cdot \frac{\eta_{ext}}{\eta_i} \cdot (R_{st} \cdot S) \tag{A-5}$$

$$= (h\nu) \cdot \frac{\eta_{ext}}{\eta_i} \cdot \frac{1}{\tau_{ph}} \cdot S \tag{A-6}$$

where $R_{st} \cdot S$ is the photons generated per unit time by stimulated emission and

$$R_{st} \approx \frac{1}{\tau_{ph}} \tag{A-7}$$

is above the threshold. The photon's lifetime, τ_{ph}, is defined as

$$\frac{1}{\tau_{ph}} = (\frac{c}{n_g}) \cdot (\alpha_s + \alpha_m) \tag{A-8}$$

where n_g is the effective group refractive index and $h\nu$ is the energy of each photon.

From equations (A-3) and (A-8), the total emitted power will be

$$P_{tot} = (h\nu) \cdot \frac{\alpha_m}{\alpha_s + \alpha_m} \cdot \left[(\frac{c}{n_g}) \cdot (\alpha_s + \alpha_m) \right] \cdot S \tag{A-9}$$

Then,

$$P_{tot} = (h\nu) \cdot \alpha_m \cdot \frac{c}{n_g} \cdot S \tag{A-10}$$

With the expression for α_m given by equation (A-2), one finally gets

$$P_{tot} = (h\nu) \cdot \frac{c}{n_g} \cdot \frac{1}{2L} \cdot \ln(\frac{1}{R_1 R_2}) \cdot S \tag{A-11}$$

where P_{tot} is the total power emitted from both facets (or both mirrors). Equation (A-11) is the relation between power (P) and photon numbers (S).

For a symmetric laser diode, a total output power P_{tot} is equal to twice of the output power per facet (P / per facet = 1/2 P_{tot}) .

Appendix B

Small signal analysis of the EC LD far above threshold can be performed by linearizing (1) and (2) with respect to small derivations around the stationary solutions and neglecting the noise terms. By inserting $S = j\omega$ into equation (32) , we get

$$\begin{aligned} D(\omega) = {} & i\omega^3 - \omega^2\left[\gamma + 2\kappa(1 - e^{i\omega\tau})\cos\phi\right] \\ & -i\omega\left[{\omega_R}^2 + \kappa^2(1 - e^{i\omega\tau})^2\right] \\ & +\kappa\left[{\omega_R}^2(1 - e^{i\omega\tau})(\cos\phi - \alpha\sin\phi)\right] \end{aligned} \qquad \text{(B-1)}$$

with $e(\tau) = 1 - e^{i\omega\tau}$, $\phi = \Omega\tau$. Then,

$$\begin{aligned} D(\omega) = {} & i\omega^3 - \omega^2\left[\gamma + 2\kappa(1 - \cos\omega\tau + i\sin\omega\tau\right]\cos\phi \\ & -i\omega\left[{\omega_R}^2 + \kappa^2(1 - 2(\cos\omega\tau + i\sin\omega\tau) + \cos 2\omega\tau + i\sin 2\omega\tau)\right] \\ & +\kappa\left[{\omega_R}^2(1 - \cos\omega\tau - i\sin\omega\tau)(\cos\phi - \alpha\sin\phi)\right] \end{aligned} \qquad \text{(B-2)}$$

For having a zero of $D(\omega)$ on the imaginary axis (the boundary of the stability), we set the real part and imaginary part of $D(\omega)$ equal to zero (Re[$D(\omega)$]=0 and Im[$D(\omega)$]=0) . The real part of $D(\omega)$ gives

$$\begin{aligned} \mathrm{Re}[D(\omega)] = {} & -\omega^2\left[\gamma + 2\kappa(1 - \cos\omega\tau)\cos\phi\right] - i\omega\left[\kappa^2(-2i\sin\omega\tau + i\sin 2\omega\tau)\right] \\ & +\kappa{\omega_R}^2(1 - \cos\omega\tau)(\cos\phi - \alpha\sin\phi) \\ = {} & -\omega^2\left[\gamma + 2\kappa(1 - \cos\omega\tau)\cos\phi\right] - \omega\left[\kappa^2(-2\sin\omega\tau + 2\sin\omega\tau\cdot\cos\omega\tau)\right] \\ & +\kappa{\omega_R}^2(1 - \cos\omega\tau)(\cos\phi - \alpha\sin\phi) \\ = {} & -\omega^2\gamma - 2\omega^2\kappa(1 - \cos\omega\tau)\cos\phi + \omega\kappa^2(-2\sin\omega\tau + 2\sin\omega\tau\cdot\cos\omega\tau) \\ & +\kappa{\omega_R}^2(1 - \cos\omega\tau)(\cos\phi - \alpha\sin\phi) \end{aligned}$$

For Re[$D(\omega)$]=0, we get

$$\begin{aligned} 0 = {} & -\omega^2\gamma - 2\omega^2\kappa(1 - \cos\omega\tau)\cos\phi + \omega\kappa^2(-2\sin\omega\tau + 2\sin\omega\tau\cdot\cos\omega\tau) \\ & +\kappa{\omega_R}^2(1 - \cos\omega\tau)(\cos\phi - \alpha\sin\phi) \end{aligned} \qquad \text{(B-3)}$$

Dividing equation (B-3) by $(\kappa{\omega_R}^2)$, we obtain

$$\begin{aligned} 0 = {} & -\frac{\omega^2}{\kappa\left(\frac{{\omega_R}^2}{\gamma}\right)} - 2\cdot\frac{\omega^2}{{\omega_R}^2}\cdot\kappa(1 - \cos\omega\tau)\cos\phi - 2\cdot\frac{\omega\kappa}{{\omega_R}^2}\cdot\sin\omega\tau \\ & +(\cos\phi - \alpha\sin\phi)(1 - \cos\omega\tau) \end{aligned} \qquad \text{(B-4)}$$

Then,

$$(1-2\cdot\frac{\omega^2}{\omega_R{}^2})(1-\cos\omega\tau)\cos\phi-\alpha\sin\phi(1-\cos\omega\tau)$$
$$=2\cdot\frac{\omega\kappa}{\omega_R{}^2}\cdot\sin\omega\tau\cdot(1-\cos\omega\tau)+\frac{\omega^2}{\kappa\omega_d} \qquad \text{(B-5)}$$

Dividing equation (B-5) by $(1-\cos\omega\tau)$ gives

$$(1-2\cdot\frac{\omega^2}{\omega_R{}^2})\cos\phi-\alpha\sin\phi=2\cdot\frac{\omega\kappa}{\omega_R{}^2}\cdot\sin\omega\tau+\frac{\omega^2}{\kappa\omega_d}\cdot\frac{1}{1-\cos\omega\tau} \quad . \qquad \text{(B-6)}$$

This is the boundary condition from the real part of $D(\omega)$.

The imaginary part of $D(\omega)$ gives ,

$$\mathrm{Im}[D(\omega)]= i\omega^3-\omega^2[2i\kappa\sin\omega\tau\cos\phi]-i\omega[\omega_R{}^2+\kappa^2(1-2\cos\omega\tau+\cos2\omega\tau)]$$
$$+\kappa[-\omega_R{}^2 i\sin\omega\tau(\cos\phi-\alpha\sin\phi)] \qquad \text{(B-7)}$$

Setting $\mathrm{Im}[D(\omega)]=0$ gets

$$\omega^3-\omega^2[2\kappa\sin\omega\tau\cos\phi]-\omega[\omega_R{}^2+\kappa^2(1-2\cos\omega\tau+\cos2\omega\tau)]$$
$$-\kappa[\omega_R{}^2\sin\omega\tau(\cos\phi-\alpha\sin\phi)]=0 \qquad \text{(B-8)}$$

Then,

$$\omega^3-\omega\omega_R{}^2=2\kappa\omega^2\sin\omega\tau\cos\phi+\omega\kappa^2(1-2\cos\omega\tau+\cos2\omega\tau)$$
$$+\kappa\omega_R{}^2\sin\omega\tau(\cos\phi-\alpha\sin\phi)$$

or

$$\omega(\omega^2-\omega_R{}^2)=2\kappa\omega^2\sin\omega\tau\cos\phi+\omega\kappa^2(1-2\cos\omega\tau+\cos2\omega\tau)$$
$$+\kappa\omega_R{}^2\sin\omega\tau(\cos\phi-\alpha\sin\phi)$$

i.e.

$$\omega(\omega^2-\omega_R{}^2)=\omega\kappa^2(1-2\cos\omega\tau+\cos2\omega\tau)$$
$$+\kappa\omega_R{}^2\sin\omega\tau\{[1-2(\frac{\omega}{\omega_R})^2]\cos\phi-\alpha\sin\phi\} \qquad \text{(B-9)}$$

By inserting equation (B-6) into RHS of equation (B-9) , we obtain

$$\omega(\omega^2-\omega_R{}^2)=\omega\kappa^2(1-2\cos\omega\tau+\cos2\omega\tau)$$
$$+\kappa\omega_R{}^2\sin\omega\tau[2\frac{\omega\kappa}{\omega_R{}^2}\cdot\sin\omega\tau+\frac{\omega^2}{\kappa\omega_d{}^2}\cdot\frac{1}{1-\cos\omega\tau}] \qquad \text{(B-10)}$$

Divided by ω, we get

$$\omega^2 - \omega_R{}^2 = \kappa^2(1-2\cos\omega\tau+\cos 2\omega\tau)$$
$$+\kappa\omega_R{}^2\sin\omega\tau[2\frac{\kappa}{\omega_R{}^2}\cdot\sin\omega\tau+\frac{\omega}{\kappa\omega_d}\cdot\frac{1}{1-\cos\omega\tau}]$$

Then,

$$\omega^2 - \omega_R{}^2 = \kappa^2(1-2\cos\omega\tau+\cos 2\omega\tau)$$
$$+2\kappa^2\cdot\sin^2\omega\tau-\frac{\omega\cdot\omega_R{}^2}{\omega_d}\cdot\frac{\sin\omega\tau}{1-\cos\omega\tau}$$

With $\omega_d = \frac{\omega_R{}^2}{\gamma}$, the damping frequency of relaxation oscillation of LD without EC , we get

$$\omega^2 - \omega_R{}^2 = \kappa^2(1-2\cos\omega\tau+\cos 2\omega\tau+2\sin^2\omega\tau)$$
$$-\frac{\omega\cdot\omega_R{}^2}{(\frac{\omega_R{}^2}{\gamma})}\cdot\frac{2\sin\frac{\omega\tau}{2}\cdot\cos\frac{\omega\tau}{2}}{2\sin^2\frac{\omega\tau}{2}} \qquad \text{(B-11)}$$

Then,

$$\omega^2 - \omega_R{}^2 = \kappa^2(2(1-\cos\omega\tau)+\cos 2\omega\tau-(1-2\sin^2\omega\tau))-\omega\gamma\cdot\cot\frac{\omega\tau}{2}$$

Using $\cos 2\omega\tau = 1-2\sin^2\omega\tau$ leads

$$\omega^2 - \omega_R{}^2 = 4\kappa^2\sin^2\frac{\omega\tau}{2}-\omega\gamma\cdot\cot\frac{\omega\tau}{2} \quad . \qquad \text{(B-12)}$$

Therefore, equations (B-6) and (B-12) show the stability boundary.

The state becomes unstable when a zero of $D(\omega)$ passes the imaginary axis. For the stable solutions the zeros of $D(\omega)$ should lie on the left side of the imaginary axis. Then we have the stability solutions in equation (33) and (34) .

Appendix C

```
/* C PROGRAM */

#include <stdlib.h>
#include <stdio.h>
#include <math.h>


#define KP     4.8        /* gain saturation coefficient  */
#define R1     0.999       /* facet reflectivity  */
#define R2     0.995       /* facet reflectivity  */
#define L      1.0e-6      /* laser cavity length */
#define NG     3.5         /* refractive index  */
#define C      3.0e8       /* light velocity   */
#define alfs       3.6e3                    /* scattering loss coefficient */
#define TSP    2.0e-9      /* spontaneous emission lifetime */
#define NS     1.41372e9       /* carrier number to reach zero gain */
#define GN     2.2e3       /* gain coefficient  */
#define A      4.0       /* linewidth enhancement factor  */
#define DL     0.0         /* simulation initial time   */
#define DH     4e-8      /* simulation final time 10ns */
#define J      0.87e18              /* injection number */
#define INTERVAL  1000         /* data printout interval   */
#define STEPS   4000000       /* steps number in (0,10ns) */


void odelong();
void rk5();
void diff();
void FB();
void nrerror();
void free_vector();
void derivs();
double *vector();

double FEXT,LEXT,TP,alpha,P;
int delay;


main()
{
long nvar, i;
double x1, x2, h1, *y;

    alpha = alfs-log(R1*R2)/(2.0*L);
    TP = NG/(C*alpha);
   P= -0.5*(6.63e-34*C/966e-9)*(log(R1*R2)/(2.0*L))*(C/NG); /*wavelengh 966nm*/
```

```
  nvar=3;
  x1=DL;
  x2=DH;


  h1=(x2-x1)/STEPS;      /* step size */

  y=vector(1, nvar);
  y[1]=1000.0;           /* y[1] I(0) */
  y[2]=0.0;              /* y[2] Q    */
  y[3]=NS;               /* y[3] N(0) */
        printf("Input the value of FEXT -=>");
        scanf("%lf",&FEXT);
        printf("Input the value of LEXT -=>");
        scanf("%lf",&LEXT);

        delay=2.0*LEXT/C/h1;

  printf(" P=%e \n", P);
  printf(" J=%e \n", J);
  printf(" delay=%d \n", delay);
  printf(" FEXT=%1.4f \n",FEXT );
  printf(" LEXT=%2.2f mm \n", LEXT*1e3);


  odelong(y, nvar, x1, x2, h1, derivs, rk5);

}


void nrerror(error_text)  /* error handle */
char error_text[];

{
   void exit();
   fprintf(stderr, " numerical run-time error ... \n");
   fprintf(stderr, "%s \n", error_text);
   fprintf(stderr, " ...exiting to system ... \n"); exit(1);
}

double *vector(nl, nh)
 long nl, nh;
/* allocates a double vector with range [ 1 .. nvar]  */
{
    double *v;
    v=(double *)malloc((unsigned) (nh-nl+1)*sizeof(double));
    if (!v)
    nrerror("allocation failure in vector()");
    return v-nl;
}
```

```
void free_vector(v, nl, nh)
double *v;
long  nl, nh;
/* frees a double vector allocated by vector()  */
{
   free((char*) (v+nl));
}


void derivs(x,  y, v, dydx)
/*  y1=S, y2=Q , y3=N
   differential equation */

double x,  y[], v[], dydx[];
{
   double CL, TO, K, temp1, ss, Q;
/*    double CL, TO, K, temp1, ss, Q, R1; */

   CL=0.5*(1-R2)/sqrt(R2);
   TO=2*L*NG/C;
   K=2*CL*sqrt(FEXT)/TO;
   temp1=GN*(y[3]-NS);

   ss=temp1*(1-KP*P*y[1])-1/TP;

   Q= -atan(A)+y[2]-v[2];


 dydx[1]=ss*y[1]+2*K*sqrt(y[1])*sqrt(v[1])*cos(Q);

 dydx[2]=0.5*A*temp1-K*sqrt(v[1])*sin(Q)/sqrt(y[1]);

 dydx[3]=J-y[3]/TSP-temp1*(1-KP*P*y[1])*y[1];

}


void odelong(ystart, nvar, x1, x2, h1, derivs, rk5)
double ystart[], x1, x2, h1;
long nvar;
void(*derivs)();    /* ANSI: void(*derivs)(double,double *,double *);  */
void(*rk5)();
/* runge-kutta integrate starting values ystart[1, nvar] from x1 to x2,
  h1 should be set as stepsize.
  derivs routine for calculate the right-hand side derivative, while rk5
  is the name of the stepper routine to be used                  */

{
   long i, k,  step;
```

```
double x, h;
double *y, *v, *dydx, *yout, *e1, *e2, *vector();
void nrerror(), free_vector();

y=vector(1, nvar);
v=vector(1, nvar-1);
dydx=vector(1, nvar);
yout=vector(1,nvar);
h=h1;

e1=vector(1, STEPS+1);     /* data storage for S(t) */
e2=vector(1, STEPS+1);     /* data storage for phase */


        printf(" h=%5.10e \n", h);
        printf(" max-step=%d \n", STEPS);
        printf(" step-delay=%d \n", delay);

for (i=1; i<=nvar; i++)
        y[i]=ystart[i];
        x=x1;
        v[1]=0.0;
        v[2]=0.0;

for (step=1; step <= STEPS; step++)  {

   e1[step]=y[1];
        e2[step]=y[2];
        if(step <= delay )
        {
        v[1]=0.0;
        v[2]=0.0;
        }
        else
        {
        v[1]=e1[step-delay];
        v[2]=e2[step-delay];
        }

        (*derivs)(x, y, v, dydx);
        rk5(y, v, dydx, nvar, x, h, e1, e2, step, yout, derivs, diff, FB);

        x=x+h;
        for (i=1; i<=nvar; i++)
        y[i]=yout[i];


 }

        e1[step]=y[1];
        e2[step]=y[2];
```

```
        x=x1;

        for (i=0; i<STEPS/INTERVAL; i++)  /* print out the datas */
        {
        k=INTERVAL*i+1;
        /* printf(" x=%e \t", x); */
        printf(" %e \t", x);
        printf(" %5.3f \n", e1[k]*P*1e3);
        x=x+INTERVAL*h;
        }

        /* printf(" x=%e \t", x); */
        printf(" %e \t", x);
        printf(" %5.3f \n", e1[k]*P*1e3);
/*      fprintf(fp," %e \t", x); */
/*      fprintf(fp," %5.3f \n", e1[k]*3.6e-5); */

        free_vector(e1, 1, STEPS+1);
        free_vector(e2, 1, STEPS+1);
        free_vector(y, 1, nvar);
        free_vector(v, 1, nvar-1);
        free_vector(yout, 1, nvar);
        free_vector(dydx,1,nvar);

}


void rk5(y, v, dydx, n, x, h, e1, e2, step, yout, derivs, diff, FB)
double y[], v[], dydx[], x, h, yout[], e1[], e2[];
void (*derivs)();     /* ANSI: void (*derivs)(double,double *,double *);  */
void (*diff)();
void (*FB)();
long n, step;
/* given values for n variables y[1,n] and their derivatives dydx[1,n] known
at x, use the fifth order Runge-Kutta method to advance the solution over
 an interval h and return the incremented variables as yout[1,n]. which need
not be a distinct array from y. the user supplies the routine derivs(x,y,dydx)
which return derivatives dydx at x. */

{
   long i;
   double *v1,*F1, *F2, *F3, *F4, *F5, *F6, *dydxt, *ytemp, *vector();
   double *S,*T;
   void free_vector();

   F1=vector(1, n);
   F2=vector(1, n);
   F3=vector(1, n);
   F4=vector(1, n);
   F5=vector(1, n);
```

```
F6=vector(1, n);
ytemp=vector(1, n);
dydxt=vector(1, n);

S=vector(1,5);
T=vector(1,5);
v1=vector(1,1);

if (step>delay)
{
 (*diff)(h,step,e1,S);
 (*diff)(h,step,e2,T);
}


for (i=1; i<=n; i++)
      F1[i]=h*dydx[i];        /* first step  */
for(i=1; i<=n; i++)
  ytemp[i]=y[i]+0.5*F1[i];


  if (step>delay)
  {
      (*FB)(0.5*h,step,S,e1,v1);
      v[1]=v1[1];
      (*FB)(0.5*h,step,T,e2,v1);
      v[2]=v1[1];
  }

      (*derivs)(x+0.5*h, ytemp, v, dydxt);   /* second step */

for(i=1; i<=n; i++)
      F2[i]=h*dydxt[i];
for(i=1; i<=n; i++)
  ytemp[i]=y[i]+0.25*F1[i]+0.25*F2[i];

      if (step>delay)
  {
      (*FB)(0.5*h,step,S,e1,v1);
      v[1]=v1[1];
      (*FB)(0.5*h,step,T,e2,v1);
      v[2]=v1[1];
  }

  (*derivs)(x+0.5*h, ytemp, v, dydxt);

for(i=1; i<=n; i++)
      F3[i]=h*dydxt[i];                /* third step */
for(i=1; i<=n; i++)
      ytemp[i]=y[i]-F2[i]+2.0*F3[i];
```

```
  if (step>delay)
  {
       v[1]=e1[step-delay+1];
       v[2]=e2[step-delay+1];
       }

       (*derivs)(x+h, ytemp, v, dydxt);
for (i=1; i<=n; i++)
       F4[i]=h*dydxt[i];                    /* fourth step */
for(i=1; i<=n; i++)
  ytemp[i]=y[i]+7.0*F1[i]/27.0+10.0*F2[i]/27.0+F4[i]/27.0;

if (step>delay)
  {
       (*FB)(2.0*h/3.0,step,S,e1,v1);
       v[1]=v1[1];
       (*FB)(2.0*h/3.0,step,T,e2,v1);
       v[2]=v1[1];
  }

 (*derivs)(x+2.0*h/3.0, ytemp, v, dydxt);

for (i=1; i<=n; i++)
       F5[i]=h*dydxt[i];                /* fifth step */

for(i=1; i<=n; i++)
  ytemp[i]=y[i]+28.0*F1[i]/625.0-0.2*F2[i]+546.0*F3[i]/625.0+54.0*F4[i]/625.0-378.0*F5[i]/625.0;

 if (step>delay)
  {
       (*FB)(0.2*h,step,S,e1,v1);
       v[1]=v1[1];
       (*FB)(0.2*h,step,T,e2,v1);
       v[2]=v1[1];
       }


  (*derivs)(x+0.2*h, ytemp, v,  dydxt);

for(i=1; i <=n; i++)
  F6[i]=h*dydxt[i];                  /* sixth step */
for (i=1; i<=n; i++)
yout[i]=y[i]+F1[i]/24.0+5.0*F4[i]/48.0+27.0*F5[i]/56.0+125.0*F6[i]/336.0;

free_vector(dydxt, 1, n);
free_vector(ytemp, 1, n);
free_vector(F6, 1, n);
free_vector(F5, 1, n);
free_vector(F4, 1, n);
free_vector(F3, 1, n);
free_vector(F2, 1, n);
```

```
   free_vector(F1, 1, n);

   free_vector(S, 1, 5);
   free_vector(T, 1, 5);
   free_vector(v1,1,1);
}


void FB(h,step,S1,S2,v1)
double h,S1[],S2[],v1[];
long  step;

/* Taylor-series expansions
  Found the feedback value between t and t+h   */
{

   v1[1]=S2[step-delay]+S1[1]*h+S1[2]*h*h/2.0+S1[3]*h*h*h/6.0+S1[4]*h*h*h*h/24.0+S1[5]*h*h*h*h*h/120.0;

 }

void diff(h,step,S3,S4)
double h,S3[],S4[];
long  step;

/* numerical differentiation :
  if step<=delay+3 : using Forward-Difference Expressions with Error of
                     Order h*h

  if step>delay+3  : using Central-difference Expressions with Error of
                     Order h*h*h*h
*/

{
   long i;

   i=step-delay;

   if(step>delay+3)
   {

   S4[1]=(-S3[i+2]+8*S3[i+1]-8*S3[i-1]+S3[i-2])/(12*h);

   S4[2]=(-S3[i+2]+16*S3[i+1]-30*S3[i]+16*S3[i-1]-S3[i-2])/(12*h*h);

   S4[3]=(-S3[i+3]+8*S3[i+2]-13*S3[i+1]+13*S3[i-1]-8*S3[i-2]+S3[i-3])
         /(8*h*h*h);

   S4[4]=(-S3[i+3]+12*S3[i+2]-39*S3[i+1]+56*S3[i]-39*S3[i-1]+12*S3[i-2]
         -S3[i-3])/(6*h*h*h*h);

   }
```

```
    else

    {
    S4[1]=(-S3[i+2]+4*S3[i+1]-3*S3[i])/(2*h) ;

    S4[2]=(-S3[i+3]+4*S3[i+2]-5*S3[i+1]+2*S3[i])/(h*h) ;

    S4[3]=(-3*S3[i+4]+14*S3[i+3]-24*S3[i+2]+18*S3[i+1]-5*S3[i])/(2*h*h*h) ;

    S4[4]=(-2*S3[i+5]+11*S3[i+4]-24*S3[i+3]+26*S3[i+2]-14*S3[i+1]+3*S3[i])
            /(h*h*h*h) ;
    }

}
```

References

1. BJARNE TROMBORG and JESPER MORK, "Nonlinear injection locking dynamics and the onset of coherence collapse in external cavity lasers," IEEE J. Quantum Electron. , vol. QE-26, pp.642-654, Apr.1990
2. J. Mork , B. Tromborg , and J. Mark , " Chaos in semiconductor lasers with optical feedback : Theory and experiments," IEEE J. Quantum Electron. , vol. 28, pp. 93-108, Jan. 1992.
3. R. Lang, and K. Kobayashi, "External optical feedback effects on semiconductor injection laser properties," IEEE J. Quantum Electron, vol. 16 , pp.347-355, Mar. 1980.
4. Alexei A. Tager and Klaus Petermann, "High frequency oscillations and self-mode locking in short external-cavity laser diodes," IEEE J. Quantum Electron. , vol.30 , pp.1553-1561, July 1994.
5. Shtengel, G., Temkin. H., and Swirhun, S.E. , "High-spped vertical-cavity surface emitting laser," IEEE Photonics Technol. Lett. , 1993, 5, (12), pp. 1359-1362
6. Petermann , Laser diode modulation and noise . Kluwer Academic Publishers, 1991.
7. Tromborg, J. H. Osmundsen, and H. Olsen, "Satbility analysis for a semiconductor laser in an external cavity," IEEE J. Quantum Electron., vol. QE-22, pp.294-301, Feb. 1986 .
8. H. Henry and R. F. Kazarinov, "Instability of semiconductor lasers due to optical feedback from distant reflectors ," IEEE J. Quantum Electron. , vol. QE-22 , pp. 294-301, Feb. 1986.
9. A. Tager and B. B. Elenkrig, "Stability regimes and high-frequency modulation of laser diodes with short external cavity," IEEE j. Quantum Electron. vol. QE-29 , pp.2886-2890, Dec. 1993 .
10. William H. Press, Brian P. Flannery, Saul A. Teukolsky and William T. Vetterling, Numerical Recipes : The art of scientific computing . Cambridge University Press 1986 .
11. David Kincaid and Ward Cheney, Numerical Analysis . Brooks/Cole Publishing company, Pacific Grove, California, 1991 .

12. Schunk and K. Petermann, "Numerical analysis of the feedback regimes for a single- mode semiconductor laser with external feedback," IEEE J. Quantum Electron., vol. 24, pp. 1242-1247 , July 1988.

☆U.S. GOVERNMENT PRINTING OFFICE: 1997-509-127-47134

MISSION OF ROME LABORATORY

Mission. The mission of Rome Laboratory is to advance the science and technologies of command, control, communications and intelligence and to transition them into systems to meet customer needs. To achieve this, Rome Lab:

a. Conducts vigorous research, development and test programs in all applicable technologies;

b. Transitions technology to current and future systems to improve operational capability, readiness, and supportability;

c. Provides a full range of technical support to Air Force Material Command product centers and other Air Force organizations;

d. Promotes transfer of technology to the private sector;

e. Maintains leading edge technological expertise in the areas of surveillance, communications, command and control, intelligence, reliability science, electro-magnetic technology, photonics, signal processing, and computational science.

The thrust areas of technical competence include: Surveillance, Communications, Command and Control, Intelligence, Signal Processing, Computer Science and Technology, Electromagnetic Technology, Photonics and Reliability Sciences.